



ELSEVIER

Contents lists available at ScienceDirect

Nuclear Instruments and Methods in
Physics Research Ajournal homepage: www.elsevier.com/locate/nima

The electromagnetic performance of the RD52 fiber calorimeter

N. Akchurin^a, F. Bedeschi^b, A. Cardini^c, M. Cascella^{d,e}, F. Ceci^{b,f}, D. De Pedis^g, R. Ferrari^h,
S. Fracchia^h, S. Franchinoⁱ, M. Fraternali^j, G. Gaudio^h, P. Genova^j, J. Hauptman^k,
L. La Rotonda^{l,m}, S. Lee^a, M. Livan^j, E. Meoniⁿ, A. Moggi^b, D. Pinci^g, A. Policicchio^{l,m},
J.G. Saraiva^o, F. Scuri^b, A. Sill^a, T. Venturelli^{l,m}, R. Wigmans^{a,*}

^a Texas Tech University, Lubbock (TX), USA^b INFN Sezione di Pisa, Italy^c INFN Sezione di Cagliari, Monserrato (CA), Italy^d Dipartimento di Fisica, Università di Salento, Italy^e INFN Sezione di Lecce, Italy^f Dipartimento di Fisica, Università di Pisa, Italy^g INFN Sezione di Roma, Italy^h INFN Sezione di Pavia, Italyⁱ CERN, Genève, Switzerland^j INFN Sezione di Pavia and Dipartimento di Fisica, Università di Pavia, Italy^k Iowa State University, Ames (IA), USA^l Dipartimento di Fisica, Università della Calabria, Italy^m INFN Cosenza, Italyⁿ Tufts University, Medford (MA), USA^o LIP, Lisbon, Portugal

ARTICLE INFO

Article history:

Received 26 June 2013

Received in revised form

29 August 2013

Accepted 10 September 2013

Available online 17 September 2013

Keywords:

Calorimetry

Cherenkov light

Optical fibers

Dual readout method

ABSTRACT

The RD52 calorimeter is an instrument intended to detect both electromagnetic and hadronic showers, as well as muons, using the dual-readout principle. Scintillation and Cherenkov light provide the two signals which, in combination, allow for superior hadronic performance. In this paper, we report on the electromagnetic performance of this instrument, and compare this performance with that of other calorimeters that were constructed with similar goals in mind.

© 2013 Elsevier B.V. All rights reserved.

1. Introduction

In most modern high-energy physics experiments, the precision with which the four-vectors of single hadrons and jets can be measured is limited by fluctuations in the energy fraction carried by the electromagnetic (em) shower component, f_{em} [1]. These fluctuations can be eliminated by simultaneous measurements of the deposited energy and the fraction of that energy carried by relativistic charged shower particles. We have experimentally demonstrated that this makes it possible to measure f_{em} event by event [2], using scintillation light and Cherenkov light as signals for the stated purposes. This method has become known as the Dual READout Method (DREAM). Since it is possible to eliminate the effects of

fluctuations in f_{em} , this method provides in practice the same advantages as intrinsically compensating calorimeters ($e/h = 1$),¹ but is not subject to the limitations of the latter devices: sampling fraction, signal integration time and volume, and especially the choice of absorber material. This has important consequences for the precision of hadronic shower measurements.

It takes a lot of material to contain the showers initiated by high-energy hadrons or jets. The RD52 Collaboration is building an optical fiber calorimeter designed to be sufficiently large to contain high-energy hadron showers at a level where leakage fluctuations no longer dominate the calorimeter performance. This detector is modular, and will eventually have an instrumented mass of about 5 tonnes.

* Corresponding author. Tel.: +1 806 742 3779; fax: +1 806 742 1182.

E-mail addresses: Richard.Wigmans@ttu.edu, wigmans@ttu.edu (R. Wigmans).¹ In an intrinsically compensating calorimeter, the response, *i.e.*, the average signal per GeV deposited energy, is equal for the em (e) and non-em (h) components of hadronic shower signals.

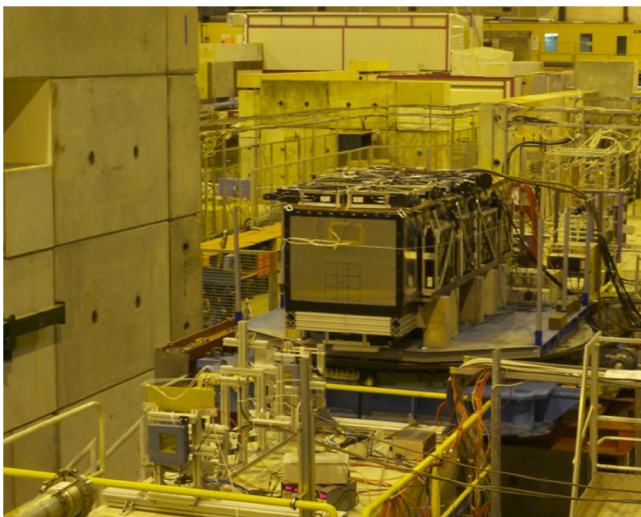


Fig. 1. The new SuperDREAM fiber calorimeter, installed in the H8C beam area. The system of trigger counters and beam defining elements is visible in the left bottom part of the figure.

Recently, a detector consisting of about one third of the final number of modules was exposed to particle beams at the CERN SPS. In this paper, we report on the electromagnetic performance of this instrument, which was large enough to contain high-energy electron and photon showers at the 99.9% level.

In Section 2, the instruments and the experimental setup in which the measurements were carried out are described, as well as the calibration and data analysis methods that were used. Experimental results are presented in Section 3. In the concluding Section 4, we discuss these results and their implications.

2. Equipment and measurements

2.1. Detectors and beam line

The measurements described in this paper were performed in the H8 beam line of the Super Proton Synchrotron at CERN. Beams of high-energy particles were steered into the RD52 fiber calorimeter. A system of auxiliary detectors, described below, was used to select electrons that entered the calorimeter in a well defined, small area. The experimental setup is shown in Fig. 1.

The fiber calorimeter is modular. Each module is 2.5 m long ($10\lambda_{\text{int}}$), and has a cross-section of $9.2 \times 9.2 \text{ cm}^2$. Each module consists of four towers ($4.6 \times 4.6 \times 250 \text{ cm}^3$), and each tower contains 1024 plastic optical fibers (diameter 1.0 mm, equal numbers of scintillating and clear fibers).² Each tower produces two signals, a scintillation signal and a Cherenkov signal, which are detected by separate PMTs.³

The first modules were constructed with lead as absorber material. In the course of 2012, we also managed to construct modules with copper as absorber material (Fig. 2). The fiducial mass of the latter was $\sim 120 \text{ kg}$, instead of 150 kg for a lead based module. One of these modules was equipped with Cherenkov fibers of which the upstream end was aluminized.⁴ Fig. 3 shows the basic structure of the modules for which lead (a) or copper

(b) was used as absorber material. In contrast with the original DREAM calorimeter [3], each fiber is now separately embedded in the absorber structure. The sampling fraction for minimum ionizing particles, both for the scintillation and for the Cherenkov sampling structure, is 5.3% for the lead-based calorimeter and 4.6% for the copper-based one.

By the end of 2012, nine lead-based modules and two copper-based ones were ready to be tested at CERN, just before the start of the two-year shutdown of the accelerator complex. These modules were assembled together, as shown in Fig. 4, and tested as such in November/December 2012.

Measurements of the radial shower profile showed that the showers initiated by 60 GeV π^- were, on average, contained at the level of 93.6% in this structure. For comparison, we mention that the average shower leakage in the original DREAM calorimeter⁵ was about 10% for 80 GeV pions. In order to detect this shower leakage, the calorimeter was surrounded by large slabs of plastic scintillator ($50 \times 50 \times 10 \text{ cm}^2$, mass 25 kg). Twenty such counters were used in these tests. They can be seen in Fig. 1 on the top, the bottom and the right hand side of the box containing the calorimeter.

In this paper, we describe the electromagnetic performance of these detectors, and shower containment was not an issue of concern for these measurements. The showers initiated by electrons sent into the center of Tower 15 were contained at the level of $\geq 99\%$, and fluctuations in shower leakage did not contribute significantly to the measured performance.

Two small scintillation counters provided the signals that were used to trigger the data acquisition system. These trigger counters were 2.5 mm thick, and the area of overlap was $4 \times 4 \text{ cm}^2$. A coincidence between the logic signals from these counters provided the trigger. The trajectories of individual beam particles could be reconstructed with the information provided by two small drift chambers, which were installed upstream and downstream of the trigger counters. This system made it possible to determine the location of the impact point of the beam particles at the calorimeter with a precision of about 1 mm. About 80 cm upstream of the calorimeter, a preshower detector (PSD) provided the signals needed to remove pions and muons contaminating the electron beams. This PSD consisted of a 5 mm thick lead plate, followed by a 5 mm thick plastic scintillator. Electrons started developing showers in this device, while muons and hadrons typically produced a signal characteristic for a minimum ionizing particle (mip) in the scintillator plate. The system of drift chambers, trigger counters and PSD can be seen in the bottom left corner of Fig. 1.

Other auxiliary detectors that were used to eliminate the hadron and muon contamination were a *tail catcher*, a $20 \times 20 \text{ cm}^2$ scintillator plate placed directly behind the calorimeter, and a $50 \times 50 \text{ cm}^2$ scintillator paddle, placed 25 m downstream, behind about 20 interaction lengths of material. The latter served as a muon counter, while hadrons typically produced signals in the tail catcher.

2.2. Data acquisition

In order to minimize delays in the DAQ system, we used special 15-mm diameter low-loss cables to transport the signals from the trigger counters to the counting room. The signal speed in these cables was measured to be 0.78c. The calorimeter signals, as well as the signals from the auxiliary counters that needed to be digitized (PSD, tail catcher, muon counter) were transported through RG-58

² The scintillating fibers were of the type SCSF-78, produced by Kuraray, the Cherenkov light was generated in PMMA based SK40 fibers, produced by Mitsubishi.

³ Hamamatsu R8900, a 10-stage 1 in. \times 1 in. PMT. The super bi-alkali photocathode covers about 85% of the outside envelope of this very compact tube.

⁴ This was done at Fermilab, by Eileen Hahn and Erik Ramberg.

⁵ That calorimeter was, in terms of nuclear interaction lengths, as deep as the present one and had a fiducial mass of 1030 kg [2].

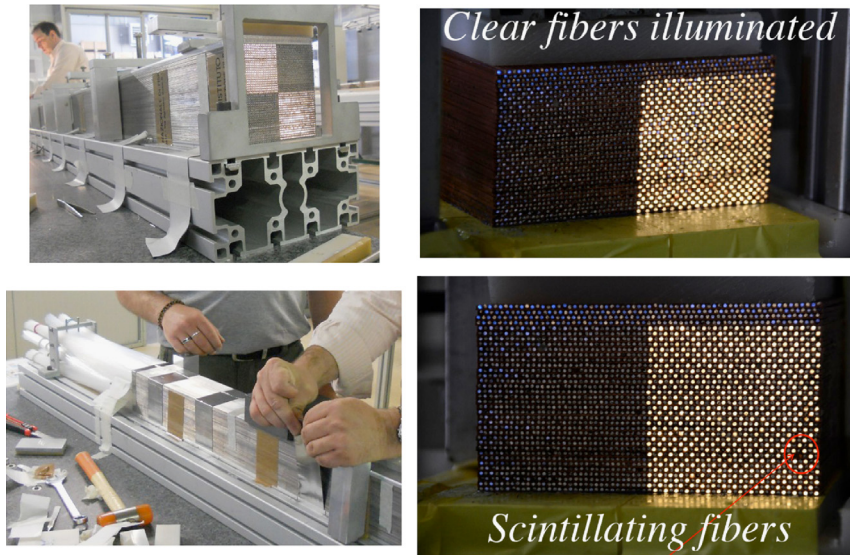


Fig. 2. Pictures of the first SuperDREAM modules built with lead (left) or copper (right) as absorber material. The alternating arrangement of clear and scintillating fibers in each row of the copper modules is illustrated by illuminating the fiber bunches from the rear end.

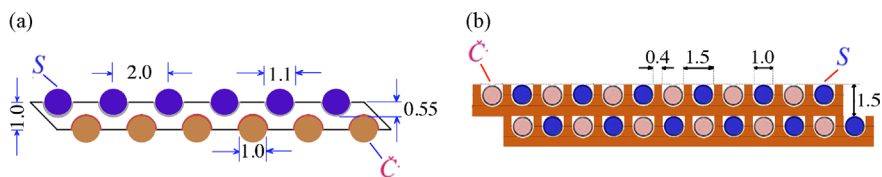


Fig. 3. Basic structure of the new lead (a) and copper (b) based RD52 fiber calorimeters.

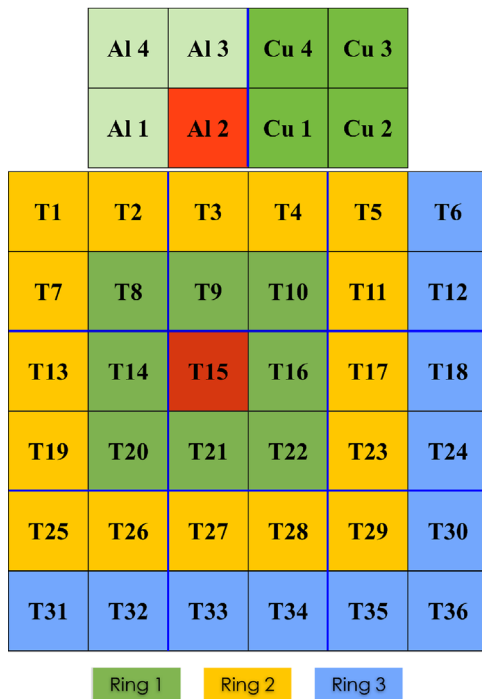


Fig. 4. The RD52 SuperDREAM calorimeter as tested at the end of 2012. It consisted of 9 lead-based modules, each consisting of 4 towers (towers 1–36), and two copper-based modules, placed on top of the lead array. The left copper module (of which the towers are marked as “Al”) is equipped with Cherenkov fibers with an aluminized upstream end face. For readout purposes, the lead calorimeter consists of a central tower (T15), surrounded by 3 square rings of towers.

cables with (for timing purposes) appropriate lengths to the counting room.

There, the signals to be digitized were fed into charge ADCs. The signals from the wire chambers were fed into TDCs. The time information could be converted into (x, y) coordinates of the point where the beam particle traversed the chamber.

The data acquisition system used VME electronics. Two VME crates hosted all the needed readout and control boards. The signals from the calorimeter channels and the auxiliary detectors were integrated and digitized with a sensitivity of 100 fC/count, on 12-bit QDC V792 CAEN modules. The timing information of the tracking chambers was recorded with 1 ns resolution in a 16-bit 16-channel CAEN V775N TDC.

Our readout scheme optimized the CPU utilization and the data taking efficiency thanks to the bunch structure of the SPS cycle, where beam particles were provided to our experiment during a spill of 9.6 s, with a repetition period of 48 s.

2.3. Experimental data and analysis methods

The measurements were performed in the H8 beam of the CERN Super Proton Synchrotron. This beam shares the particle production target (T4) with another beam (H6), which means in practice that the momentum (as well as the charge sign) of secondary particles available to us depended on the measurement program in this other beam line. The electron beams were derived from secondary beams at 80 GeV and 180 GeV. The beam particles were sent through a 5 mm thick lead radiator. In practice, only the electron component of the secondary beam lost a substantial energy fraction passing through this material, and electrons of the desired momentum were selected with

properly tuned downstream bending magnets. In this way, electron beams of 6, 10, 20, 30, 40 and 60 GeV were derived from the 80 GeV secondary beam, while the 180 GeV secondary beam formed the source of electron beams at 60, 80, 100, 125 and 150 GeV.

Because of the existing boundary conditions, the high-energy electrons could only be used to test the 36-tower lead-based matrix, while the lower-energy electrons were used to test the copper modules.

The measurements of the signal linearity and the em energy resolution were performed by steering the electron beams into the center of Tower 15 (lead), or in the center of Tower A12 (copper, see Fig. 4). Typically, for each energy 50 000 events were collected, although that number could either be considerably lower (limited by the count rate, at the lowest energies) or higher (to overcome substantial contamination, at the highest energies). For reasons explained in Section 3.6, the calorimeter was oriented at a small angle with the beam line during these measurements: 1.5° in the horizontal plane (we will refer to this angle as θ), 1.0° in the vertical plane (this one will be called ϕ).

In each run, 10% randomly triggered events provided pedestal information. For each event, the ADC information of all calorimeter towers was recorded, as well as the ADC (and in some cases also TDC) data from the auxiliary detectors (muon counter, wire chambers, PSD, tail catcher).

Other measurements were carried out to determine the uniformity of the calorimeter response. We used 100 GeV electrons to measure the uniformity of the lead modules, and 20 GeV electrons for the copper ones. In these measurements, the calorimeter was perfectly aligned with the beam line, *i.e.*, the angle between the fibers and the beam particles was 0° . The measurements were carried out by systematically mapping the calorimeter response to these particles over an extended surface area. In the case of the lead modules, an area of $9 \times 9 \text{ cm}^2$ centered on the 4-corners point of Towers 15, 16, 21 and 22 (see Fig. 4) was studied for this purpose, with a total of 650 000 beam particles. In the case of the copper modules, an area of $6 \times 2 \text{ cm}^2$ covering the central regions of Towers A12 and A11, as well as the four-corners region, was exposed to 150 000 electrons of 20 GeV.

Off-line, the beam chamber information could be used to select events that entered the calorimeter in a small (typically $10 \times 10 \text{ mm}^2$) region located around its geometric center. The electron beams contained some fraction of muons and hadrons, which could be effectively eliminated with the PSD, the tail catcher and the downstream muon counter. The hadron contamination was largest at the highest energies, the muon contamination was also important at the lowest energies.

Fig. 5 shows the effects of these cleanup procedures for the 125 GeV beam.

2.4. Calibration

The calibration of the calorimeter towers was performed with 20 GeV electrons. A beam of these electrons, selected to form a $20 \times 20 \text{ mm}^2$ beamspot by means of the beam chambers, was steered into the centers of each of the 36+8 calorimeter towers. In the first iteration of the calibration procedure, the average signals, expressed in ADC counts, were equalized for all towers. In the next step, the energy deposited in the hit tower was determined, as follows. We used tower 15, which was the tower in which the beams were steered for all energy scans in the lead structure, for this purpose. The signals from tower 15 and from all other towers constituting rings 1, 2 and 3 (Fig. 4) were added together, in terms of ADC counts. Subsequently, the total number of ADC counts was defined as 20 GeV, and this formed the basis for the calibration constants of all towers.

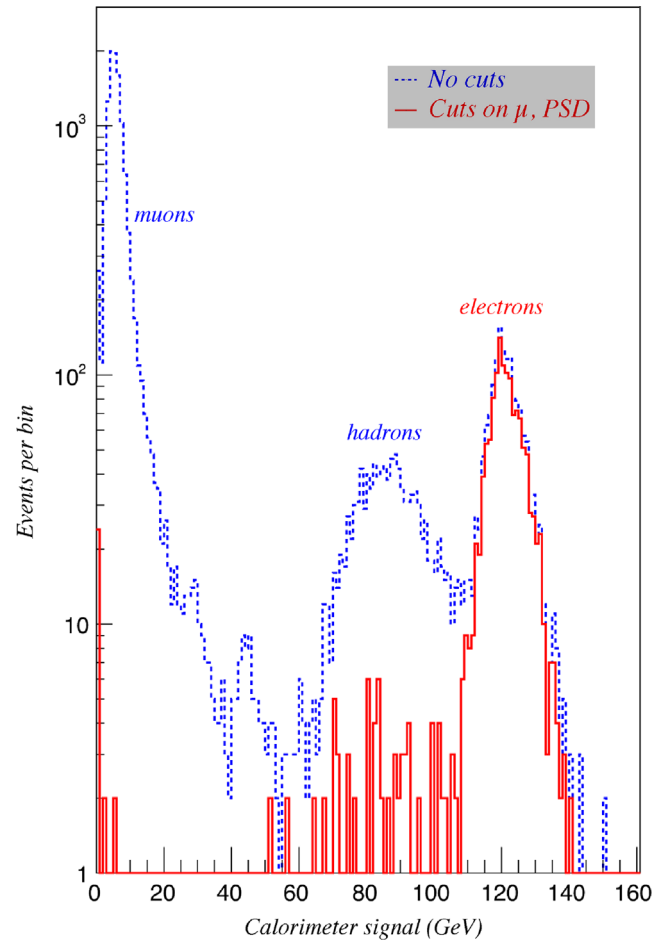


Fig. 5. Signal distributions for the 125 GeV beam before and after the cuts intended to obtain pure electron event samples.

It turned out that the electrons deposited, on average, 85% of their energy in the central tower (#15 in this case), the rest was distributed over the other 35 towers. The average signals observed in the hit towers during the calibration runs thus corresponded to 17 GeV, for both types of signals, and the calibration constants were calculated accordingly, in terms of GeV per ADC count.

The electrons deposited a small fraction of their energy in the preshower detector. The scintillation counter that was part of the PSD provided a measure of this energy loss, event by event. Fig. 6a shows a typical signal distribution measured by this counter.

The mip peak contains contributions from pions and muons that contaminated the beam. The peaks at 3 mips and 5 mips are the result of energetic photons radiated by the electrons and converting in the lead. Beam electrons were defined as particles that produced a signal larger than the indicated cutoff value in the PSD.

The energy scale of the PSD signals was determined from the anti-correlation between these signals and the ones produced by the same particles in the fiber calorimeter. Fig. 6b shows this anti-correlation very clearly, for 10 GeV electrons. The energy scale of the PSD signals was set by requiring that the sum of both signals be constant. The average energy loss in the PSD was found to be 0.27 GeV, for 10 GeV electrons. As the beam energy increased, so did the average energy loss in the PSD. At 60 GeV, it was found to be, on average, 0.36 GeV. Monte Carlo simulations based on GEANT4 confirmed these findings. According to these simulations, the losses were caused by two mechanisms: absorption of soft Bremsstrahlung γ s in the PSD itself (a) and Bremsstrahlung γ s that

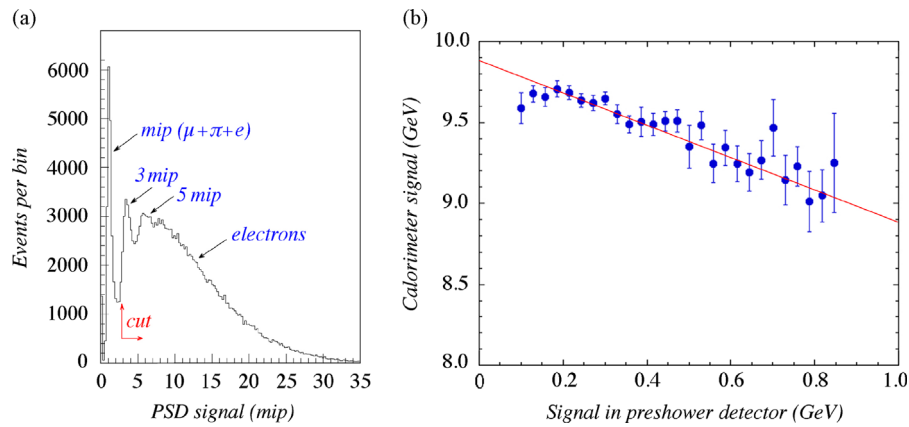


Fig. 6. Typical signal distribution in the preshower detector (a), and the correlation between the signals in this detector and in the calorimeter (b).

exited the PSD at such an angle that they missed the calorimeter (b). Including the measured PSD signals improved both the calorimeter resolution and the signal linearity somewhat, especially at the lowest energies.

3. Experimental results

3.1. The electromagnetic response function

The electron response was obtained by adding the signals from all available towers that contributed to it. The signal from each contributing tower was converted into energy by means of the calibration constants, whose values were determined as described in Section 2.4. In the case of the lead module, the signals from all 36 towers were used for this purpose. The beam was steered into the center of Tower 15. The signal from that tower contributed typically $\sim 85\%$ to the total energy. Ring 1 (*i.e.*, the 8 towers numbered T8, 9, 10, 14, 16, 20, 21, 22, see Fig. 4) contributed in total $\sim 12\%$ and the 16 towers constituting Ring 2 (see Fig. 4) contributed together $\sim 2.5\%$ to the total calorimeter signal. Finally, the 11 towers from the incomplete ring 3 contributed together $\sim 0.5\%$. Since the radial profile of em showers is in principle energy independent [1], these numbers may also be considered representative for electron showers at other energies.

The total signals thus consisted of the sum of 36 individual contributions, and since most of these contributions were very small, one might wonder if adding all these tiny contributions from outlying towers did more than just adding electronic noise (because of pedestal fluctuations) to the total signal. Fig. 7 shows the sum of the signals from the 12 towers constituting ring 2. The total energy deposited in these 12 towers was, on average, 0.472 GeV. For comparison, the distribution of the sum of the pedestals from all 36 towers is shown in the same figure. The energy equivalence of the width of this total pedestal distribution was 0.098 GeV. Therefore, pedestal fluctuations (*i.e.*, electronic noise) contributed only 1.0% to the resolution at 10 GeV and 0.1% at 100 GeV. Given the fact that this contribution is added in quadrature to the contributions of other fluctuations, it is fair to say that it was in practice negligible.

For the total signal from the copper calorimeter, we only considered the tower into which the electron beam was steered (Tower A12, see Fig. 4), as well as one ring of towers surrounding this tower. Based on the numbers mentioned above, this means that typically 97% of the total shower energy was deposited in this ensemble. It should be mentioned that in this case also the signals from 3 lead-based towers (T2, 3, 4, see Fig. 4) were taken into account. However, since these towers typically contributed less than 5% to the total response, this

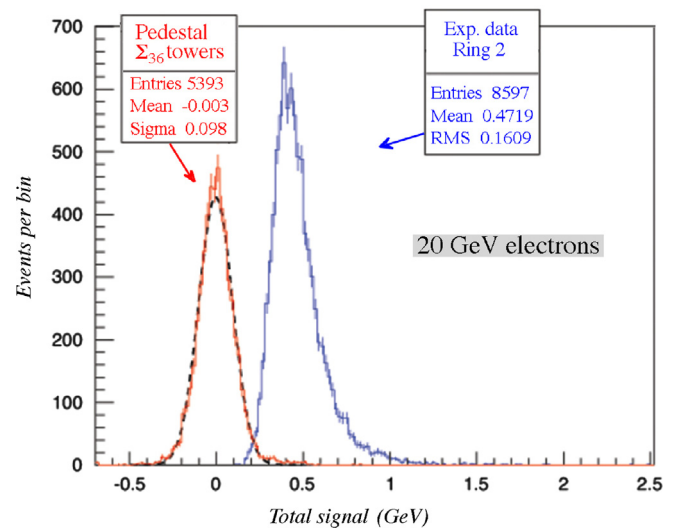


Fig. 7. Distribution of the contribution of the scintillation signals from ring 2 to the total signal from 20 GeV electrons steered into the center of Tower 15. For comparison, the distribution of the sum of the pedestals in all 36 towers contributing to the signal is shown as well.

was not considered an unacceptable contamination of the results quoted for “copper”.

We also added the signals from the preshower detector to the total calorimeter signal, calibrated as described in Section 2.4. The signal distributions obtained in this way were well described by Gaussian functions. In the following, we use the mean values and standard deviations obtained from such fits as the experimental results of our studies. As an example, Fig. 8 shows the response functions plus the results of the fits for electrons of 40 GeV in the copper based fiber calorimeter. The scintillation and Cherenkov signal distributions are shown separately in Fig. 8a and b, respectively. These signals were also summed together for each event. The resulting signal distribution for these summed signals, shown in Fig. 8c, is considerably narrower than the individual distributions for each fiber type. The nearly exact factor of $\sqrt{2}$ between the individual resolutions for the two types of fibers (Fig. 8a and b) and the resolution for their summed signals (Fig. 8c) indicates that we have achieved statistical independence of each fiber type.

3.2. Signal linearity

Intrinsic signal linearity for em shower detection is a very fundamental calorimetric property, not only for homogeneous detectors, but for *all types* of calorimeters. This is because the entire em

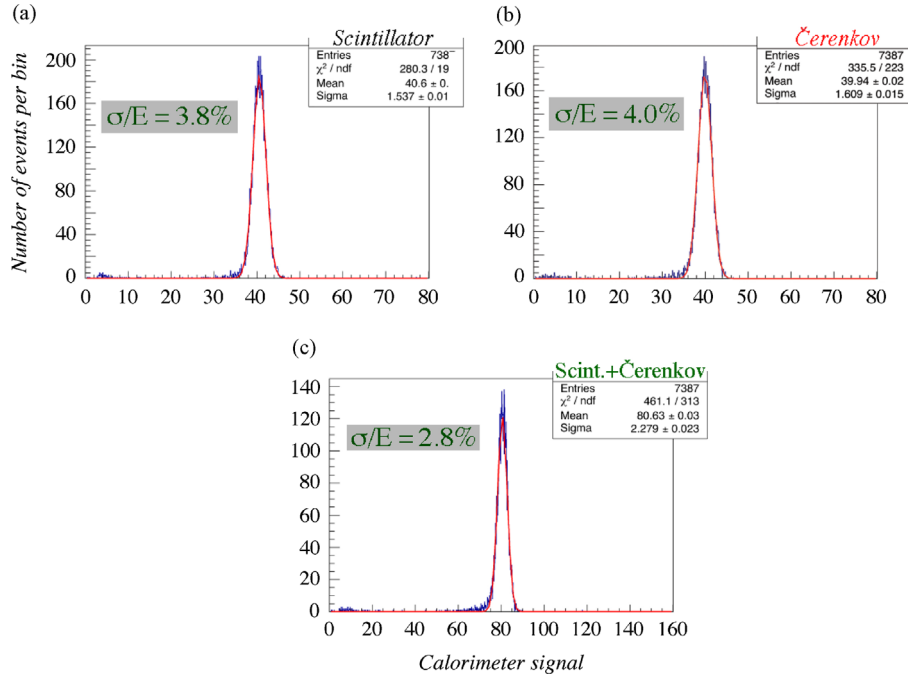


Fig. 8. Signal distributions for 40 GeV electrons in the copper-fiber calorimeter. Shown are the distributions measured with the scintillating fibers (a), the Cherenkov fibres (b) and the sum of all fibers (c). The angle of incidence of the beam particles (θ , ϕ) was $(1.5^\circ, 1.0^\circ)$. The size of the beam spot was $10 \times 10 \text{ mm}^2$.

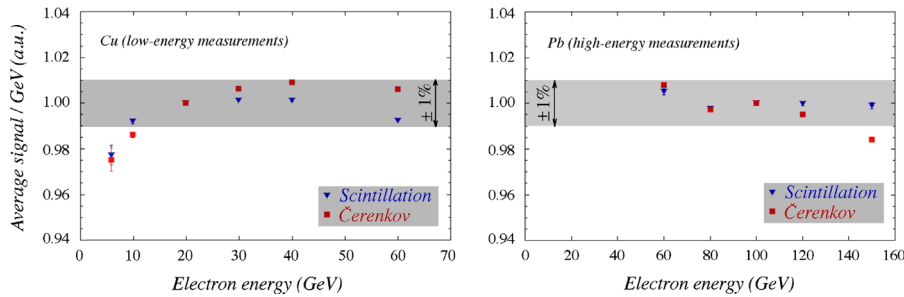


Fig. 9. The linearity of the copper (a) and lead (b) based fiber calorimeters for em shower detection in the scintillation and Cherenkov channels. See text for details.

shower energy is used to ionize the absorbing medium, in contrast with hadronic showers where some (variable) fraction of the shower energy is used to break up atomic nuclei, or escapes detection altogether. When deviations from linearity are observed for em calorimeters, these are invariably caused by instrumental effects, such as saturation effects in the active media or in the readout, incomplete shower containment, upstream absorption effects, inactive or inefficient volumes, etc.

Because of the logistics of the data taking procedures (see Section 2.3), the signal linearity was studied over two energy ranges: 6–60 GeV and 60–150 GeV, respectively. Fig. 9 shows the calorimeter response, defined as the average signal per unit deposited energy, separately for the scintillation signals and for the Cherenkov signals in these two energy ranges. The response is constant to within 1% (i.e., the gray area in these figures) in both ranges, with the exception of the lowest energy point (6 GeV), where the response is about 2% lower than average. At these low energies, the reconstructed energy is most sensitive to energy losses upstream. Apart from the PSD, the electrons also lose some energy in the other upstream detectors (trigger counters, wire chambers), in 10 m of air, beam pipe windows, etc. In addition, backscattering of soft photons through the front face of the calorimeter (so-called *albedo* effects) are also most important for low-energy showers. And finally, hysteresis effects in the beam magnets, which affect the precise energy of the beam particles, are most important at low energies as well.

In any case, the fiber calorimeter is linear for em shower detection to within $\pm 1\%$, over the energy range 10–150 GeV, both for the scintillation and the Cherenkov signals.

3.3. Radial shower profiles

It is well known that the radial profiles of electromagnetic showers are very narrow, especially in the early phase, before the shower maximum is reached [5]. In that phase, the shower development is dominated by energetic Bremsstrahlung photons radiated by the beam particle, and these γ s convert into e^+e^- pairs that travel close and parallel to the shower axis. In order to assess the effects of this on the performance of our calorimeter, we measured this shower profile, in the following way. We used a run in which a wide beam of 100 GeV electrons was steered into the boundary region of Towers 15 and 16. The beam particles entered the calorimeter parallel to the direction of the fibers ($\theta, \phi = 0^\circ$). We selected events in a 1 mm wide sliver of this beam spot and moved this area in small steps across the boundary between the two towers, as illustrated in the insert of Fig. 10.

Fig. 10a shows the signal measured in Tower 16 as a function of the position of this sliver, separately for the scintillation and Cherenkov signals. The very steep increase of the signal near the boundary between towers 15 and 16 is indicative for the very narrow shower profile. This profile can be extracted from these

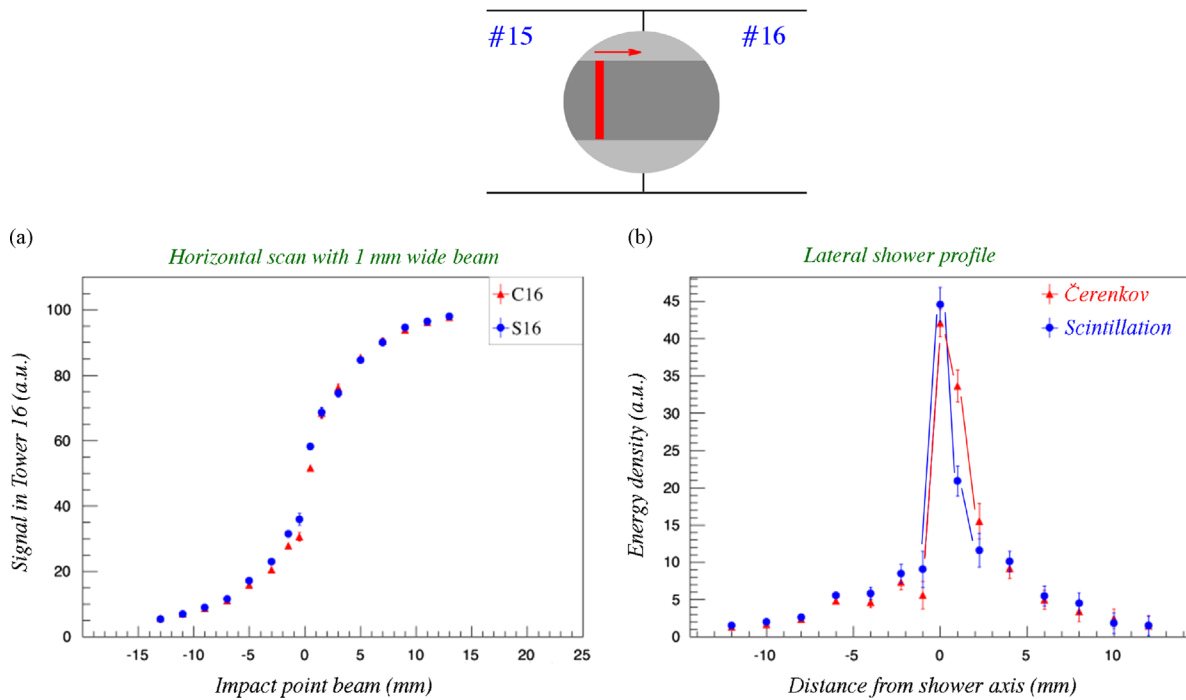


Fig. 10. The signal from a 1 mm wide beam of 100 GeV electrons measured in Tower 16, as a function of the impact point of the beam (a), and the lateral shower profiles derived from this measurement (b). See text for details.

measurements by taking the derivative of this curve. In Fig. 10b, the differences between the signals measured at neighboring impact points are plotted. This figure shows that the narrow central core of the showers extends over a distance of only a few mm. The core is somewhat wider for the Čerenkov signals than for the scintillation ones.⁶

Because of the extremely collimated core of the em showers, there is a systematic response difference between particles entering the detector in the absorber material or in the fibers for this type of calorimeter. The core is more efficiently sampled, and thus contributes more to the total signal, when it develops in or very close to a fiber. By orienting the calorimeter at a small angle with respect to the beam line, this difference is smeared out and eventually disappears for angles $\gtrsim 3^\circ$ [3,4]. Interestingly, this effect is more or less absent for the Čerenkov signals. This is because the extremely collimated narrow core that characterizes the early phase of em showers does *not* contribute to the Čerenkov signals, since the Čerenkov light generated in this phase falls outside the numerical aperture of the fibers [3]. We come back to these effects in Section 4.

3.4. Response uniformity

Because of the extremely collimated core of the em showers, a large contribution of the signals comes from a very small number of individual fibers. This means that it is very important that fiber-to-fiber response variations be kept as small as possible. Such variations may be caused by:

- Differences in intrinsic fiber quality (light yield, attenuation characteristics).
- Differences in the quality of the polishing of the fiber ends.

- Differences in quantum efficiency of the PMT photocathode areas illuminated by individual fibers.

In order to investigate these effects, we performed *uniformity scans*, in which a relatively large area of the calorimeter surface was exposed to a given electron beam. In order to maximize the effects of non-uniformities, the calorimeter was oriented at $\theta, \phi = 0^\circ$, so that the number of fibers contributing to the signal from individual showers was made as small as possible. To obtain a fine granularity, a large number of beam particles were used for this study, which was carried out with 100 GeV electrons for the lead matrix and with 20 GeV electrons for the copper modules. The granularity, *i.e.*, the size of the individual cells into which the scanned surface area was subdivided, was $5 \times 5 \text{ mm}^2$ in the case of lead, and $2 \times 2 \text{ mm}^2$ for copper.

Results are given in Fig. 11 for the lead matrix and Fig. 12 for the copper modules. We want to emphasize that the fibers and PMTs were identical for these two scans. Yet, some striking differences were observed. In general, the uniformity is worse for the lead modules than for the copper ones, which may be partly due to the fact that the lead scan included a larger fraction of areas near the tower edges.⁷ Especially for the scintillation signals in the lead matrix, there is a substantial difference between the response to particles that hit a tower in its center and particles that entered the calorimeter near a tower edge. No such difference was observed for copper. Also, the Čerenkov response in lead was much more uniform than the scintillation response (7% vs. 12% non-uniformity). This is consistent with the fact, explained in the previous subsection, that the Čerenkov signals are less sensitive to anomalies in one individual fiber, since the early extremely collimated shower component does not contribute to these signals.

⁶ This phenomenon is due to the fact that the early, extremely collimated part of the shower does *not* contribute to the Čerenkov signal, since the Čerenkov light generated in this stage falls outside the numerical aperture of the fibers [6].

⁷ In order to quantify this effect, we also limited the study of the signal variations in the lead calorimeter to the same areas that were included in the copper scan. The non-uniformity was measured to be 11% and 6% for the scintillation and the Čerenkov signals, respectively.

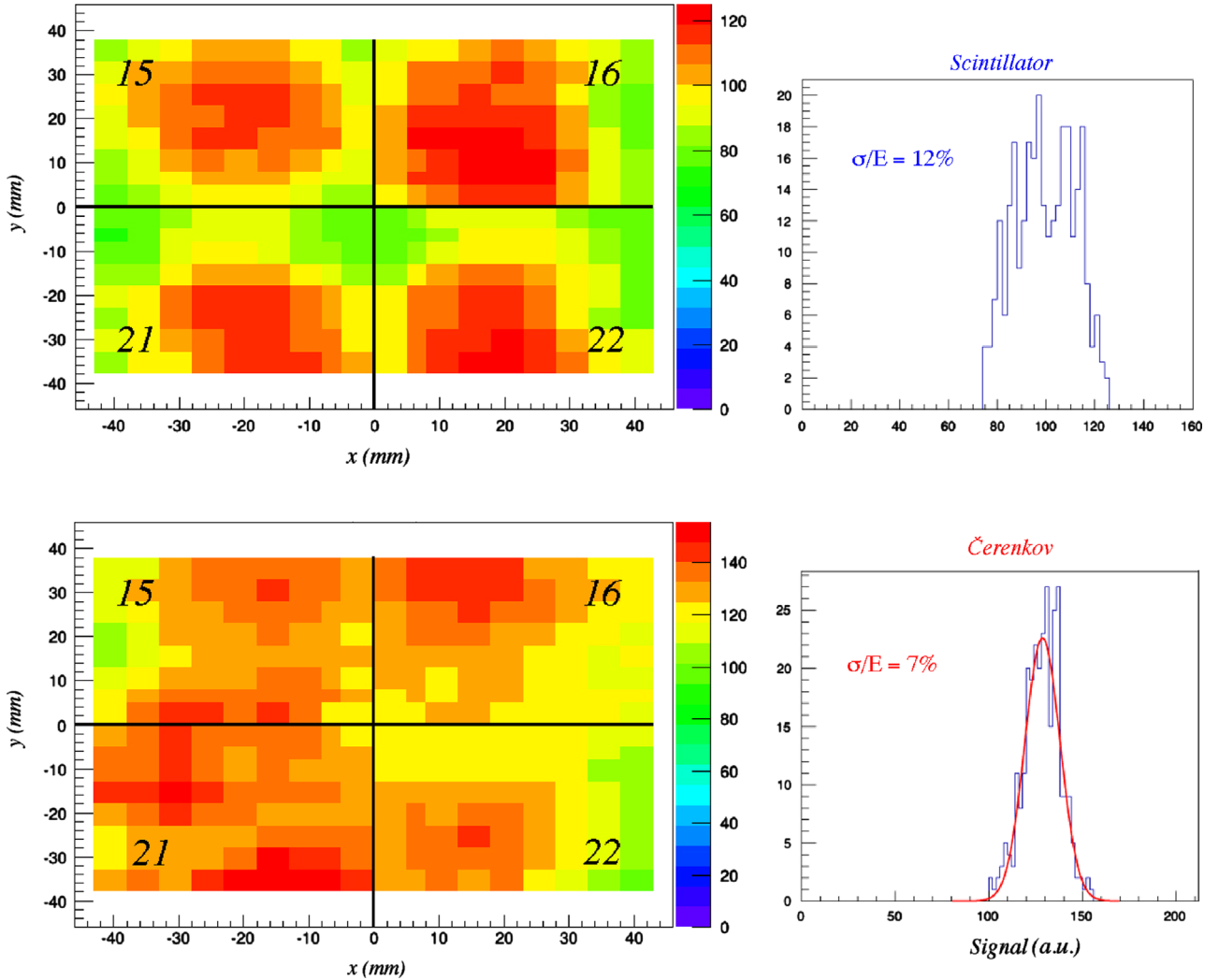


Fig. 11. Uniformity scan of the central region of the lead matrix with 100 GeV electrons. Results are given in the form of a response map (left) or a histogram (right), separately for the scintillation (top) and the Cherenkov signals (bottom). See text for details.

The copper results seem to contradict the latter conclusion, since the non-uniformity was in that case measured to be larger for the Cherenkov signals compared to the scintillation ones. Yet, one should keep in mind that the upstream ends of the Cherenkov fibers were aluminized in that module, in an attempt to increase the light yield. This was not done for the scintillating fibers. Fiber-to-fiber variations in the reflection coefficient of the upstream fiber ends may very well have introduced an additional source of non-uniformity.

The origins of the observed non-uniformities clearly need to be better understood. The differences between the lead and copper results seem to indicate that differences in the fiber polishing procedures might have played a role. Also, it is probably a good idea to use light mixers between the fiber bunches and the PMT surface. This would make the results much less sensitive to local variations in the quantum efficiency of the photocathode.

Yet, as we will show in the next subsection, the effects of the measured non-uniformities on the electromagnetic energy resolutions are much smaller than suggested by the results shown in Figs. 11 and 12. Also, we want to emphasize that the observed non-uniformity effects are unlikely to play any significant role at all for hadron detection, because the numbers of fibers that contribute to the signals from individual showers is much larger than for em showers, so that fiber-to-fiber response variations have much smaller effects. Also, the energy resolution for hadron

detection is typically about twice as large as for electrons in this type of calorimeter.

3.5. The electromagnetic energy resolution

For the measurements of the em energy resolution, the calorimeter was oriented at a small angle with the beam line, 1.5° in the horizontal plane (θ), 1.0° in the vertical plane (ϕ). This is an efficient way to reduce the effects discussed in the previous subsections, since it reduces the contributions of individual fibers to the overall calorimeter response. The effects induced by the position dependence of the calorimeter response are, in good approximation, independent of the electron energy. This is true both for the effects resulting from the extremely collimated early shower component (Section 3.3), and for the effects deriving from fiber-to-fiber response variations (Section 3.4). As we will see, the experimental energy resolution data make it possible to distinguish between these two types of contributions, both of which lead to a deviation from $E^{-1/2}$ scaling (usually referred to as a “constant term”). Therefore, the effects manifest themselves primarily at the highest energies.

We first look at the data obtained with the copper calorimeter. The energy resolutions were measured for electrons ranging from 6 to 60 GeV in this device. The results are shown in Fig. 13, where the resolution is given as a function of energy, which is plotted on

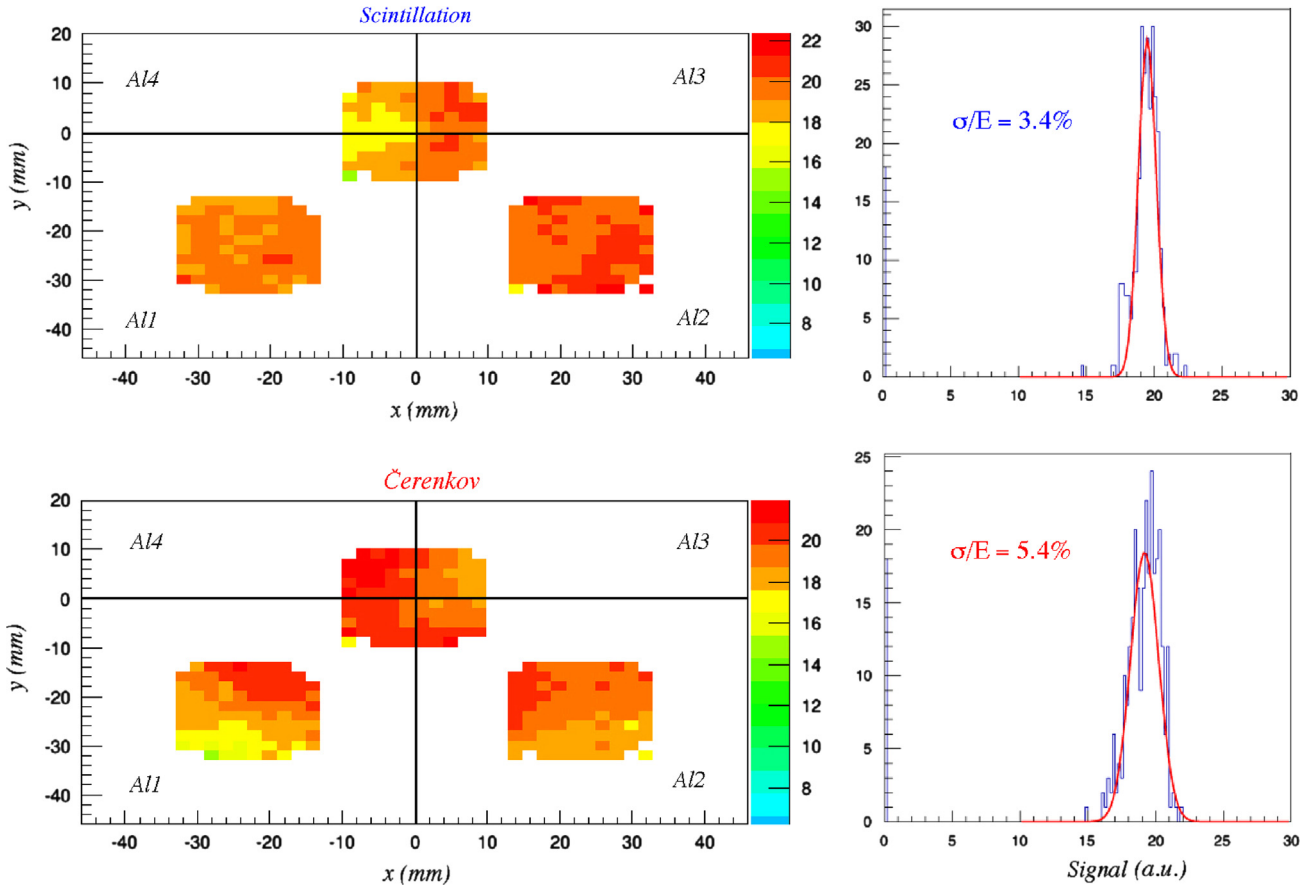


Fig. 12. Uniformity scan in the aluminized copper module with 20 GeV electrons. Results are given in the form of a response map (left) or a histogram (right), separately for the scintillation (top) and the Čerenkov signals (bottom). See text for details.

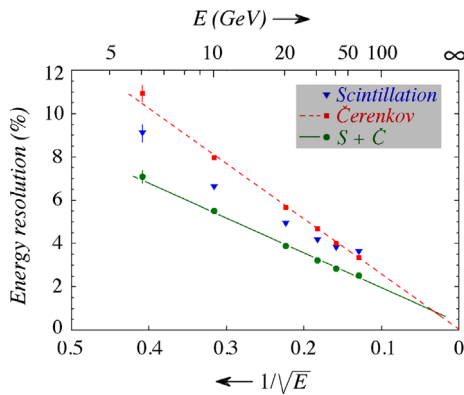


Fig. 13. The energy resolution for electrons in the copper-fiber module, as a function of the beam energy. Shown are the results for the two types of fibers, and for the combined signals. The angle of incidence of the beam particles (θ , ϕ) was (1.5° , 1.0°). The size of the beam spot was $10 \times 10 \text{ mm}^2$.

a scale that is linear in $E^{-1/2}$. Represented in this way, scaling with $E^{-1/2}$ is thus represented by a straight line through the bottom right corner of the plot. The experimental data for the Čerenkov signals are indeed well described by such a line. On the other hand, the resolution for the scintillation signals clearly contains a deviating component, which we estimate to be at the level of 2%–3%. One effect of this constant term is that the energy resolution at 60 GeV is even better for the Čerenkov signals than for the scintillation ones. Since the response uniformity is even better for the latter signals (see Fig. 12), we conclude that this deviation must be caused by the effects described in Section 3.3. Despite the very fine sampling, the scintillation calorimeter response is still

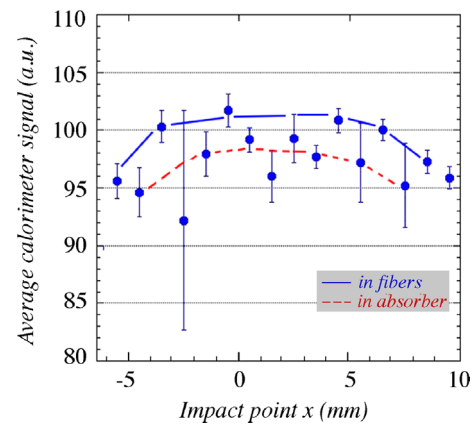


Fig. 14. The scintillation signal for 100 GeV electrons developing showers in the lead matrix as a function of the impact point of the beam particles. See text for details.

affected by the extremely collimated early shower component and thus depends on the impact point of the beam particles: inside a fiber or inside the absorber separating the fibers.

We tried to find support for the conclusion that even in this very fine sampling calorimeter, the scintillation signal depends on the impact point of the electrons, *i.e.*, inside a scintillating fiber or in the absorber material separating these fibers. This was done in the lead matrix, which should not make a difference in this respect since the fiber structure was very similar (see Fig. 3). A beam of 100 GeV electrons was steered into the center of Tower 15. We selected a sliver of 1 mm in x and 15 mm in the y coordinate and looked at the average scintillation signal as this sliver was moved

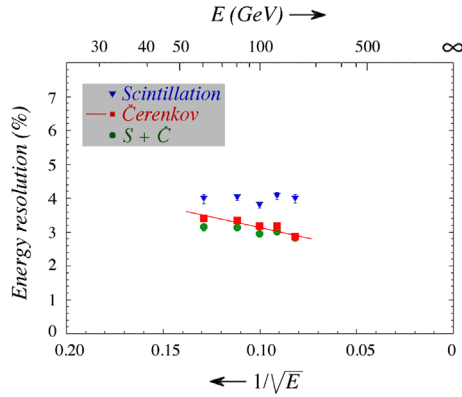


Fig. 15. The energy resolution for electrons in the lead-fiber module, as a function of the beam energy. Shown are the results for the two types of fibers, and for the combined signals. The angle of incidence of the beam particles (θ , ϕ) was $(1.5^\circ, 1.0^\circ)$. The size of the beam spot was $10 \times 10 \text{ mm}^2$.

across the central region of this tower. The results are shown in Fig. 14, which exhibits indeed an oscillating pattern with a period of about 2 mm, *i.e.*, the distance between two scintillating fibers. Over a distance of 14 mm, one can indeed see the expected number of maxima and minima (seven). The average difference between the maximum and minimum signals is about 4%, *i.e.*, consistent with a constant term of $\sim 2\%$ in the em energy resolution.

One advantage of the new fiber pattern used in the RD52 calorimeters is the fact that the scintillation and Cherenkov read-out represent completely independent sampling structures. Therefore, by combining the signals from the two types of fibers, a significant improvement in the energy resolution is obtained. This was not the case for the original DREAM calorimeter [3], where the two types of fibers essentially sampled the showers in the same way. Fig. 13 shows that the energy resolution of the combined signal deviates slightly from $E^{-1/2}$ scaling. The straight line fit through the data points suggests a constant term of 1% or less. In any case, the energy resolution is substantially better than for either of the two individual signals, over the entire energy range covered by these measurements.

We now turn to the results of the energy resolution measurements in the lead matrix, shown in Fig. 15. These measurements were carried out with electrons ranging in energy from 60 to 150 GeV. The figure shows that the resolution of the scintillation signals is approximately constant, at $\sim 4\%$, while the resolution for the Cherenkov signals slightly improves with energy, and is definitely better than that measured for the scintillating fibers. Yet, the improvement does not scale with $E^{-1/2}$ and there is thus also in this case a contribution from a non-stochastic term.

Since there is no reason why the effects from the collimated early shower component should be any different from that measured in the copper structure, we conclude that in this case also the fiber-to-fiber response variations contribute to the measured energy resolution, for both types of fibers. This conclusion is consistent with the fact that such fluctuations were measured to be much larger in the lead matrix (Fig. 11).

It is also interesting to note that, in contrast with the copper results, combining the two signals does *not* lead to a significant improvement of the energy resolution for the lead matrix. This means that sampling fluctuations, which contribute to the stochastic term, are a minor component of the measured resolution, which is dominated by response non-uniformities. Additional evidence for this can be derived from Fig. 16a, which shows the energy resolution for 80 GeV electrons as a function of the size of the beam spot. As the beam spot is reduced from the standard size of $10 \times 10 \text{ mm}^2$, the energy resolution improves significantly, by

$\sim 25\%$. This means that the resolutions measured for the standard beam spot size contain a contribution from response non-uniformities in the form of an energy independent term of $\sim 2\%$. The results shown in Fig. 15 would thus have looked much better if a much smaller beam spot had been used in the data analysis. Fig. 16b shows that no such dependence on the size of the beam spot was observed in the case of the copper measurements.

3.6. Angular dependence of the response

Given the fact that the performance of this calorimeter is sensitive to the angle of incidence of the beam particles, one may wonder what happens if particles enter this calorimeter at larger angles. It was demonstrated long ago that the response of a scintillating-fiber calorimeter is independent of the angle of incidence [1], but since the emission of Cherenkov radiation is a directional phenomenon, this may be very different for this calorimeter. The fact that the Cherenkov fibers are insensitive to the early, extremely collimated shower component, is a strong indication in this respect. If the calorimeter would be oriented such that the Cherenkov light emitted in this early shower phase was trapped within the numerical aperture of the Cherenkov fibers, a considerably larger signal might be expected.

We tested this hypothesis in an earlier stage, with measurements on an individual (lead based) prototype module of the RD52 calorimeter. This module was exposed to a beam of electrons of 80 GeV. The response of the eight signals in the four towers was equalized when the beam entered the calorimeter at θ , $\phi = 0^\circ$, just as in the measurements described earlier in this paper. Next the module was rotated in the horizontal plane and the calorimeter signals were measured as a function of the angle of incidence, θ . For angles larger than 10° , the particles entered the module from the side. The resulting average signals measured in the scintillation and Cherenkov channels are shown in Fig. 17. Since the module has a transverse width of only $9X_0$, the signals decreased as the angle increased. However, the angular dependence of the two types of signals was clearly very different. This is illustrated in more detail in Fig. 18, where the Cherenkov/scintillation signal ratio is plotted as a function of the angle of incidence, separately for the two towers that contributed to the signals (see Fig. 17).

As expected, the signal ratio increases with the angle, to reach a maximum at $\theta = 51^\circ$, where the acceptance for Cherenkov light emitted by shower particles traveling parallel to the beam line is largest.⁸ The increase with respect to the ratio that was established when calibrating the module was measured to be $\sim 65\%$ for the first tower traversed by the particles (T4), and $\sim 50\%$ for the second one (T1). This decrease is of course due to the fact that the latter tower (T1) sees a somewhat less collimated shower than T4. The asymmetry seen in T1 is due to the fact that the shower component measured by this tower depends on the angle of incidence. For example, at $\theta = 20^\circ$, T1 probes the shower at a depth ranging from 13 to $26X_0$, at $\theta = 50^\circ$ from 6 to $12X_0$ and at $\theta = 70^\circ$ from 4 to $8X_0$. Therefore, the large-angle portions of the data points in Fig. 18a and b are much more similar than the rest, since at large angles both towers probe the early stage, before the shower maximum.

However, despite the angular dependences, the figures also show that the Cherenkov/scintillation signal ratio is approximately constant in the angular range $\theta = 0^\circ - 10^\circ$. In a practical

⁸ The Cherenkov fibers used in this prototype module were based on polystyrene, which has an index of refraction $n=1.59$, which corresponds to a Cherenkov angle of 51° . The modules that constitute the RD52 calorimeter contain Cherenkov fibers based on PMMA ($n=1.49$), which has much better light attenuation characteristics in the relevant wavelength region.

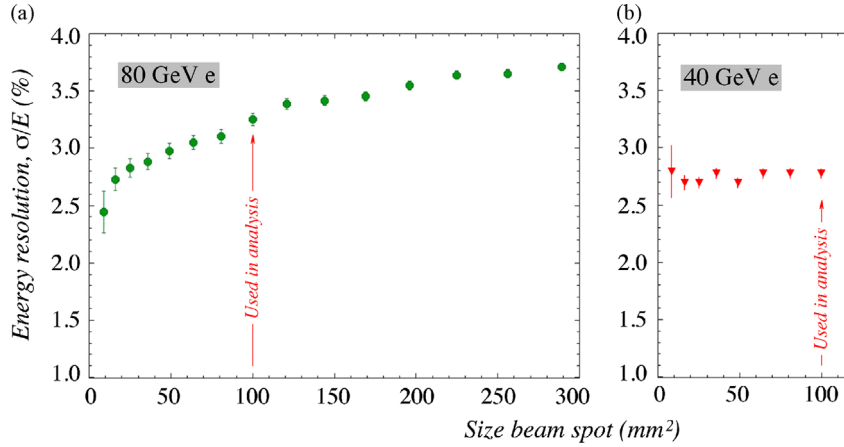


Fig. 16. The energy resolution as a function of the size of the beam spot. Shown are the results for the combined scintillation and Cherenkov signals for 80 GeV electrons in the lead calorimeter (a) and for 40 GeV electrons in the copper module (b).

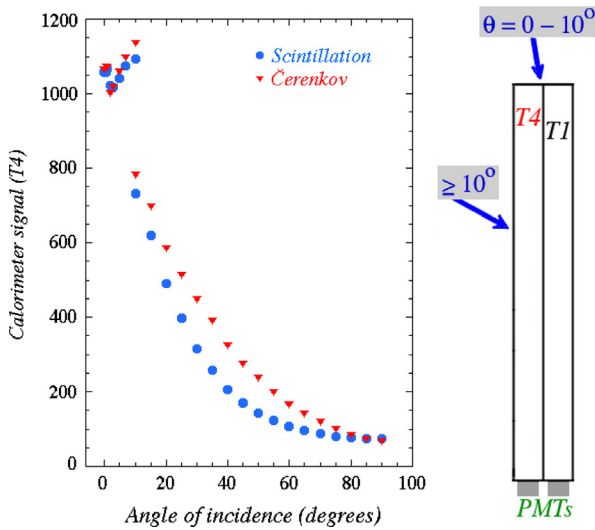


Fig. 17. The average scintillation and Cherenkov signals as function of the angle of incidence of the 80 GeV electrons used for this study. The insert shows the geometry of the exposed module and the direction of incidence of the beam particles. These measurements were performed with an earlier lead-based prototype module. See text for details.

experiment, the calorimeters will most likely be constructed in such a way that the most energetic particles, *i.e.*, the dominating jet components, enter the detector always in this angular range.⁹

3.7. The light yield

A very important (and limiting) characteristic of this type of calorimeter is the Cherenkov light yield. Together with the sampling fluctuations, fluctuations in the numbers of photoelectrons (p.e.) determine the stochastic term in the energy resolution. In order to determine the number of photoelectrons produced per unit of deposited shower energy (N_{GeV}), we need to know the absolute gain of the PMT, for the light spectrum produced by the

fibers in question. Once that gain (G) is known, N_{GeV} can be determined from the charge produced in the ADC per unit energy deposited in the calorimeter (Q_{GeV})

$$Q_{\text{GeV}} = 1.6 \times 10^{-19} N_{\text{GeV}} G. \quad (1)$$

We measured the gain of the PMTs using a blue LED as the light source. This diode produced light with a wavelength of 481 nm, representative for the light produced by our fibers. The light pulses produced by this LED¹⁰ were sent through optical fibers to two separate PMTs, one of which served as reference to monitor the stability of the source. The light pulses were shaped electronically to resemble those produced by the showers developing in the calorimeter. The intensity of the light pulses could be varied by means of the voltage applied to the diode. Typical light levels chosen for these measurements produced between 20 and 200 photoelectrons per pulse in the PMT. The precise value of the light level was determined from the variance in the PMT signals, which was dominated by photoelectron statistics.

These measurements were carried out with a digital oscilloscope, which recorded for each pulse the integrated pulse height (in pV s). Divided by the input impedance of the oscilloscope, this gave the integrated output charge for each pulse. And since the charge of the input signal was known from the average number of photoelectrons produced, the gain of the PMT was simply determined by

$$G = Q_{\text{out}}/Q_{\text{in}}. \quad (2)$$

Measurements of the PMT gain and, therefore, of the light yield (N_{GeV}) were carried out for the scintillation and Cherenkov signals of towers 15, 16 and 21 of the lead matrix and tower A1 2 of the copper module (Fig. 4). The light yield was measured to be in the range of 100–200 photoelectrons per GeV deposited energy for the scintillation channels, and 20–40 photoelectrons per GeV for the Cherenkov channels. Differences between the results obtained for individual towers are mainly attributed to differences in the quantum efficiency of the PMT which converts the light into electric signals, in the quality of the polishing of the fiber ends and in the optical coupling between the fiber bundles and the PMT windows.

⁹ The angular width of distributions such as the ones shown in Fig. 18 is determined by the numerical aperture of the fibers. Reducing the index of refraction from 1.59 to 1.49 narrows the angular width of the bump and increases the angular range for which the responses of the Cherenkov and scintillation structures are about equal [7].

¹⁰ A 5 mm SiC diode, manufactured by Hewlett Packard. The rise time and FWHM of the pulses were set to 5 ns each.

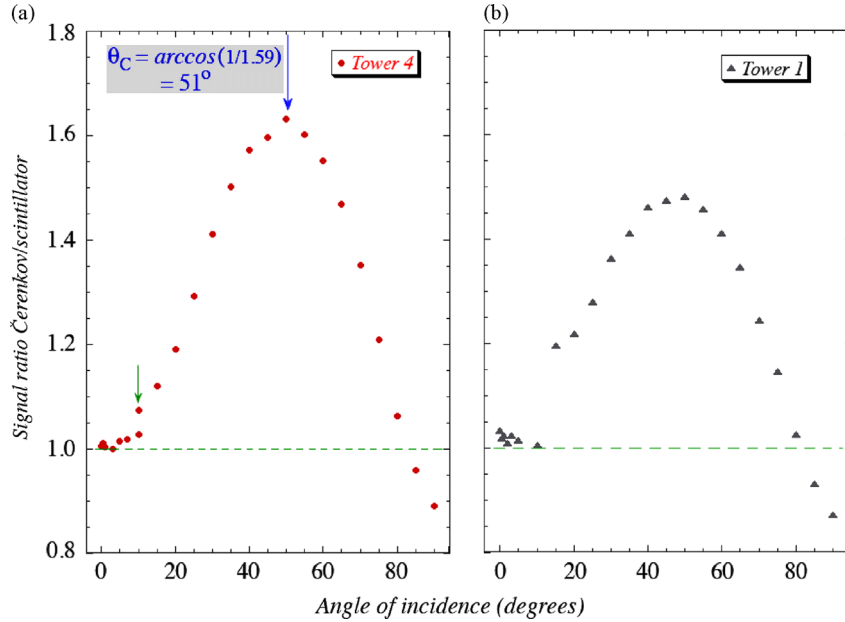


Fig. 18. The Cherenkov/scintillation signal ratio for 80 GeV electrons as a function of the angle of incidence of the beam particles with respect to the fiber direction. The results are given for the first (a) and second (b) tower traversed by the particle showers. The setup of these measurements is shown in Fig. 17.

4. Discussion

4.1. Decomposition of the measured energy resolution

In well designed calorimeters, stochastic fluctuations dominate the em energy resolution. Contributions come from sampling fluctuations and from fluctuations in the numbers of photoelectrons produced per GeV deposited energy

$$\frac{\sigma}{E} = \frac{a_{\text{stoch}}}{\sqrt{E}} \quad \text{with } a_{\text{stoch}} = a_{\text{samp}} \oplus a_{p.e.} \quad (3)$$

Sampling fluctuations are determined both by the sampling fraction and the sampling frequency, i.e., both by the fraction of the shower energy deposited in the active calorimeter layers, and by the dimensions of these individual sampling layers. The following empirical formula was found to describe sampling fluctuations in a large variety of different sampling calorimeters using non-gaseous active material [8]:

$$a_{\text{samp}} = 0.027 \sqrt{d/f_{\text{samp}}}, \quad (4)$$

in which d represents the thickness of individual active sampling layers (in mm), and f_{samp} the sampling fraction for minimum ionizing particles (*mips*). In our copper module, $d=1.0$ mm and $f_{\text{samp}}=0.046$, so that $a_{\text{samp}}=0.127$. Based on the measured light yield, we found for the contributions of fluctuations in the numbers of photoelectrons for the scintillation and Cherenkov channels in this module ($a_{p.e.}=1/\sqrt{N_{\text{GeV}}}$) values of 0.103 and 0.189, respectively. This leads to expected stochastic terms $a_{\text{stoch}}=0.227$ for the Cherenkov channel and 0.162 for the scintillation channel.

These results are graphically depicted in Fig. 19, where the experimental data points are the same ones as in Fig. 13. The contributions of sampling fluctuations and the total stochastic fluctuations are represented by the dashed and solid lines, respectively. Apart from the results for the Cherenkov (Fig. 19a) and scintillation signals (Fig. 19b), Fig. 19c shows the results for the combined signals. In that case, the sampling fluctuations are reduced by a factor $\sqrt{2}$, to 8.9%, while the total stochastic term becomes 13.9%.

Fig. 19 shows that the slopes of the solid lines (describing the total stochastic term) are very similar to the slopes of the experimental data. Deviations from $E^{-1/2}$ scaling are largest in the case of the scintillation signals, and smallest for the Cherenkov ones. These deviations are caused by effects discussed earlier in this paper, in particular signal non-uniformities which cause the response to depend on the impact point of the particles. Since the beam spot used for the lowest energy particles (6 GeV) was larger than for the other energies, it stands to reason that the deviation from $E^{-1/2}$ scaling is somewhat larger than average at this energy (see also Fig. 16 in this context).

The figure also illustrates to what extent the energy resolution might be further improved by increasing the light yield. A further increase, e.g., through light detectors with a larger quantum efficiency might improve the total resolution possibly by as much as 30%. Additional gains may be obtained by eliminating or reducing the effects of response non-uniformities.

4.2. Comparison with other integrated fiber calorimeters

An important characteristic of the RD52 calorimeter is the fact that, while it is *longitudinally unsegmented*, it is intended to measure all particles (electrons, gammas, hadrons and jets) with the same instrument, calibrated with electrons. Previously, two other fiber calorimeters based on the same idea have been constructed and tested: SPACAL and DREAM. It is therefore interesting to compare the em performance of the RD52 calorimeter with that of these two instruments, whose results are described in Refs. [4,3], respectively.

Fig. 20 shows the differences in the sampling structures of the three calorimeters, on the same scale. The sampling fraction of SPACAL was dictated by compensation requirements, which did not play a role for the other two calorimeters, whose structure was instead affected by the properties of the PMTs which were used to detect the light signals. In the DREAM calorimeter, which was the first one to test the dual-readout principle, the two types of fibers were housed together in the same hollow copper tubes. The two types of fibers were split at the rear end of the module. As a result, they sampled the showers that developed in the calorimeter in the same way, and the energy resolution did not improve when both

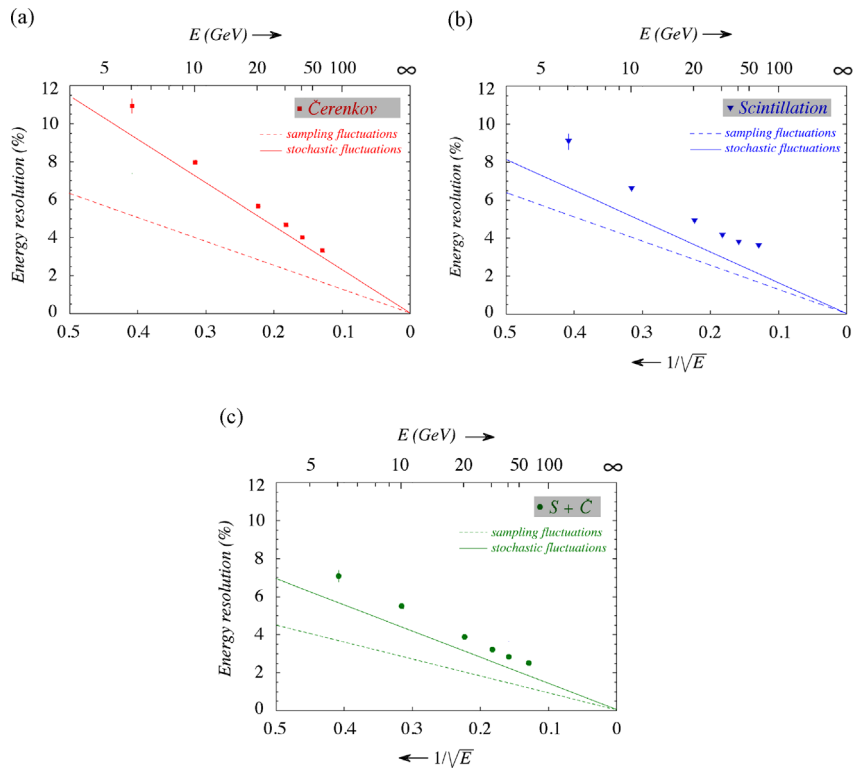


Fig. 19. The em energy resolution measured with the Cherenkov fibers (a), the scintillating fibers (b) and the sum of all fibers (c) in the copper-fiber calorimeter. Also shown are for each case the contributions of sampling fluctuations and the total stochastic fluctuations. The latter are defined as the quadratic sum of sampling fluctuations and Poisson fluctuations in the number of photoelectrons. See text for details.

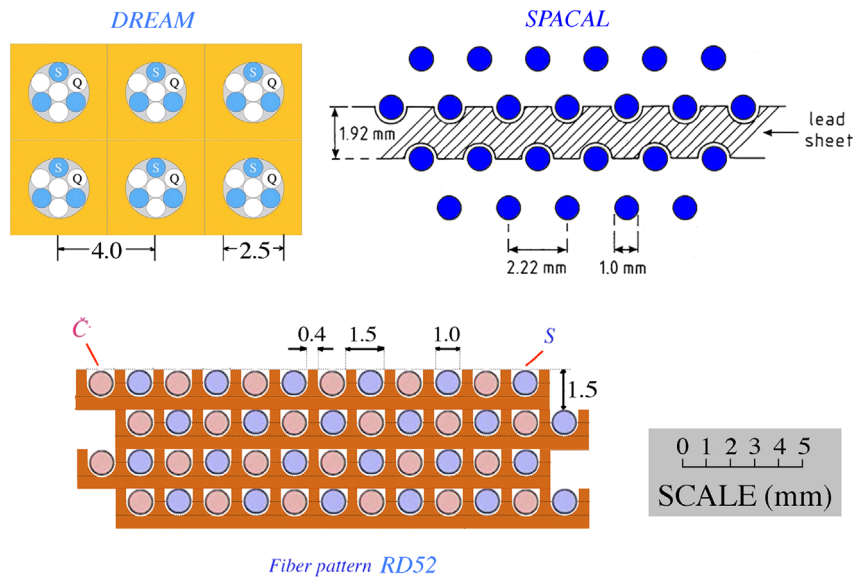


Fig. 20. The structure of the new RD52 calorimeter (copper-based modules), compared to that of two other fiber calorimeters: DREAM [3] and SPACAL [4].

signals were combined. In that sense, the RD52 structure led to a big improvement, as illustrated in Fig. 13.

Because of the extremely collimated core of the em showers, there is a systematic response difference between particles entering the detector inside the absorber material or inside the fibers in this type of calorimeter. This difference is responsible for a non-Gaussian line shape of the scintillation signals, which is clearly visible in the DREAM calorimeter (Fig. 21c). This effect gets rapidly worse when the angle of incidence of the particles approaches 0°. As explained in Section 3.3, this effect is absent for the Cherenkov signals, which are even in the

rather crudely sampling DREAM calorimeter well described by a Gaussian function (Fig. 21d).

Because of the very small distance between neighboring sampling layers (fibers), this impact point dependence barely affects the lineshape of the RD52 calorimeter.¹¹ This is illustrated

¹¹ Expressed in Moliere radii (ρ_M), the distance between neighboring fibers is $0.022\rho_M$ in RD52, $0.099\rho_M$ in DREAM and $0.071\rho_M$ in SPACAL.

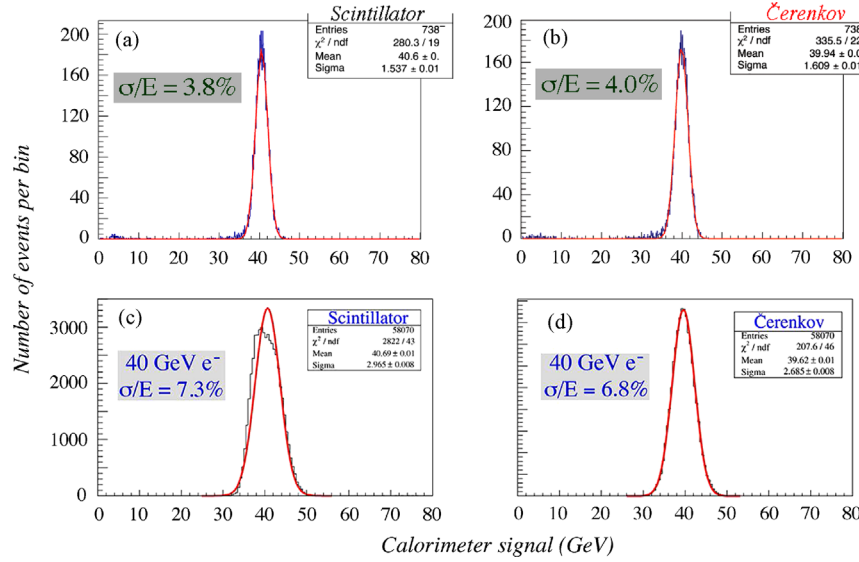


Fig. 21. Comparison of the em response functions measured with the RD52 copper-fiber calorimeter and the original DREAM copper-fiber calorimeter [3], for 40 GeV electrons. Results are given separately for the scintillation and Cherenkov signals.

in Fig. 21a and b. Yet, the resolution measured with the scintillation signals does show a deviation from $E^{-1/2}$ scaling (Fig. 13).

Apart from the lineshape, such deviations are also indicative for the mentioned impact point dependence of the energy resolution. The immunity of the Cherenkov signals in this respect is illustrated by the fact that no deviation of $E^{-1/2}$ scaling was observed for the Cu-fiber RD52 calorimeter. The energy resolutions measured with the more crudely sampling DREAM and SPACAL calorimeters all exhibited significantly larger deviations from $E^{-1/2}$ scaling. As illustrated in Fig. 22, this was even true for the resolution measured for the Cherenkov signals in DREAM.

In interpreting the results shown in this figure, it is important to realize that, apart from differences in construction, there were also differences in the angle at which the electrons entered the different calorimeters during the tests. In that sense, it is important that the results shown for the DREAM and SPACAL calorimeters were obtained at considerably larger angles than the ones for the RD52 calorimeter. For example, the DREAM results were obtained for angles $\theta = 3^\circ$, $\phi = 2^\circ$. In this geometry, the resolution extrapolated to values of 1.5% and 1.1% at $E = \infty$ for the scintillation and Cherenkov signals, respectively. If the angles were reduced to $\theta = 2^\circ$, $\phi = 0.7^\circ$, the constant term for the scintillation signals increased to 5.6%, while that for the Cherenkov signals remained essentially unchanged [3]. The latter geometry is much closer to the one in which the RD52 calorimeter was tested ($\theta = 1.5^\circ$, $\phi = 1.0^\circ$, respectively). Therefore, it is fair to say that the change in geometry has led to a very substantial improvement in the electromagnetic performance.

4.3. Evaluation of the RD52 results

The RD52 dual-readout calorimeter was primarily designed to offer superb performance for hadron and jet detection, made possible by the combination of scintillation and Cherenkov signals. The instrument of which tests are described in this paper was too small to verify this goal experimentally. Yet, our tests do show that the same instrument is also a very good detector of electromagnetic showers.

Fig. 22 shows that at energies above 20 GeV, the em energy resolution is better than that of any of the other integrated fiber calorimeters. Further improvements may be expected when response non-uniformities due to fiber-to-fiber variations, which especially affect the scintillation signals, can be eliminated. Better fiber polishing procedures, in combination with the use of light mixers, are foreseen

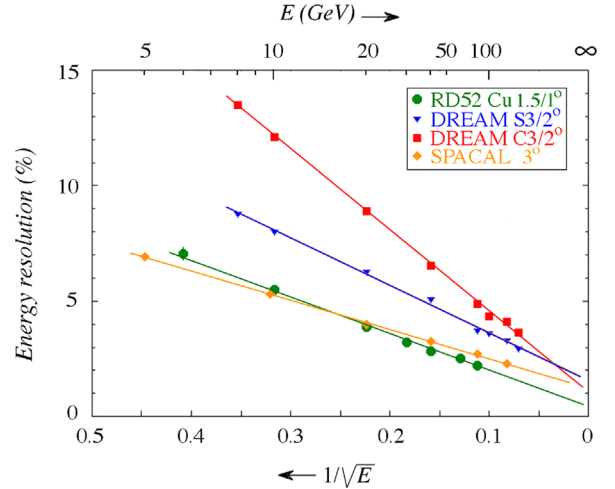


Fig. 22. Comparison of the em energy resolution measured with the RD52 copper-fiber calorimeter, the original DREAM copper-fiber calorimeter [3], and the SPACAL lead-fiber calorimeter [4].

to this end. We want to emphasize again that this most probably will not make any significant difference for the hadronic performance. Because of the large number of fibers that typically contribute to hadronic signals, these are insensitive to the fiber-to-fiber response variations that affect the electromagnetic signals.

The results also show that even better resolutions may be expected for particles that enter the detector at angles larger than the 1.5° used in these tests. In future tests, we plan to carry out a systematic study of the angular dependence of the performance. We are also planning to use high-energy collider data to see what is the experimental angular distribution of high-energy electrons and γ s entering the calorimeter, in order to assess if special precautions would have to be taken in the design of an instrument of this type for a 4π experiment.

Acknowledgments

We thank CERN, and in particular Dr. Ilias Efthymiopoulos and Michael Jeckel for making particle beams available to our experiments

in the H8 beam. We gratefully acknowledge Eileen Hahn and Erik Ramberg of Fermilab who took care of the aluminization of the Cherenkov fibers used in one of the copper modules. This study was carried out with financial support of the United States Department of Energy, under contract DE-FG02-12ER41783, and by Italy's Istituto Nazionale di Fisica Nucleare and Ministero dell'Istruzione, dell'Università e della Ricerca.

References

- [1] R. Wigmans, *Calorimetry, Energy Measurement in Particle Physics, International Series of Monographs on Physics*, vol. 107, Oxford University Press, 2000.
- [2] N. Akchurin, et al., *Nucl. Instr. and Meth. A* 537 (2005) 537.
- [3] N. Akchurin, et al., *Nucl. Instr. and Meth. A* 536 (2005) 29.
- [4] D. Acosta, et al., *Nucl. Instr. and Meth. A* 308 (1991) 481.
- [5] N. Akchurin, et al., *Nucl. Instr. and Meth. A* 548 (2005) 336.
- [6] N. Akchurin, et al., *Nucl. Instr. and Meth. A* 533 (2004) 305.
- [7] N. Akchurin, R. Wigmans, *Rev. Sci. Instr.* 74 (2003) 2955.
- [8] R. Wigmans, in: C. Grupen, I. Buvat (Eds.), *Handbook of Particle Detection and Imaging*, vol. 1, Springer Verlag, 2011, pp. 497–517.